# Monomer–dimer dynamics and distribution of GPI-anchored uPAR are determined by cell surface protein assemblies

Valeria R. Caiolfa,[1,2] Moreno Zamai,[1,2] Gabriele Malengo,[1,3] Annapaola Andolfo,[4] Chris D. Madsen,[4] Jason Sutin,[5] Michelle A. Digman,[5] Enrico Gratton,[5] Francesco Blasi,[1,3,4] and Nicolai Sidenius[1,4]

[1]Department of Molecular Biology and Functional Genomics and [2]Italian Institute of Technology Network Research, Unit of Molecular Neuroscience, San Raffaele Scientific Institute, 20132 Milano, Italy
[3]Università Vita-Salute San Raffaele, 20132 Milano, Italy
[4]Fondazione Italiana per la Ricerca sul Cancro Institute of Molecular Oncology, 20139 Milano, Italy
[5]Laboratory for Fluorescence Dynamics, University of California, Irvine, Irvine 92697, CA

To search for functional links between glycosylphosphatidylinositol (GPI) protein monomer–oligomer exchange and membrane dynamics and confinement, we studied urokinase plasminogen activator (uPA) receptor (uPAR), a GPI receptor involved in the regulation of cell adhesion, migration, and proliferation. Using a functionally active fluorescent protein–uPAR in live cells, we analyzed the effect that extracellular matrix proteins and uPAR ligands have on uPAR dynamics and dimerization at the cell membrane. Vitronectin directs the recruitment of dimers and slows down the diffusion of the receptors at the basal membrane. The commitment to uPA–plasminogen activator inhibitor type 1–mediated endocytosis and recycling modifies uPAR diffusion and induces an exchange between uPAR monomers and dimers. This exchange is fully reversible. The data demonstrate that cell surface protein assemblies are important in regulating the dynamics and localization of uPAR at the cell membrane and the exchange of monomers and dimers. These results also provide a strong rationale for dynamic studies of GPI-anchored molecules in live cells at steady state and in the absence of cross-linker/clustering agents.

## Introduction

The oligomerization of glycosylphosphatidylinositol (GPI)-anchored membrane proteins is thought to regulate their association with membrane domains (lipid rafts), their subcellular sorting, and their biological function (Simons and Toomre, 2000; Mayor and Riezman, 2004; Paladino et al., 2004). However, little is known about the connection between oligomerization, microdomain confinement, and membrane dynamics of GPI-anchored proteins in their resting but functionally active state in living cell in the absence of artificial clustering agents such as chemical cross-linkers or antibodies.

Correspondence to Valeria R. Caiolfa: valeria.caiolfa@hsr.it; or Francesco Blasi: francesco.blasi@hsr.it

Abbreviations used in this paper: ACF, autocorrelation function; cpsm, counts per second per molecule; FCS, fluorescence correlation spectroscopy; FLIM, fluorescence lifetime imaging microscopy; Fn, fibronectin; FRET, Förster resonance energy transfer; GPI, glycosylphosphatidylinositol; mRFP, monomeric RFP; PAI1, plasminogen activator inhibitor type 1; PCH, photon-counting histogram; TCSPC, time-correlated single-photon counting; uPA, urokinase plasminogen activator; uPAR, uPA receptor; Vn, vitronectin; wt, wild type.

The online version of this article contains supplemental material.

To address these issues, we have chosen to study the urokinase plasminogen activator (uPA) receptor (uPAR) because it mediates a wide range of cellular events (for review see Blasi and Carmeliet, 2002). uPAR is involved in the regulation of diverse physiological and pathological processes, including cell adhesion and migration as well as angiogenesis, tumor invasion, metastasis, and proliferation. It is generally accepted that uPAR-mediated events involve the binding and proteolytic activity of uPA; however, uPAR also mediates events that do not require uPA and entail transmembrane signaling, regulating adhesion and chemotactic movement of myeloid cells (Gyetko et al., 1994), migration of epithelial and endothelial cells (Busso et al., 1994; Odekon et al., 1994), and cell proliferation (Liu et al., 2002).

As for other GPI proteins, the dynamic exchange in membrane microdomains (Kusumi and Suzuki, 2005; Lenne et al., 2006) may explain the involvement of uPAR in signal transduction processes. However, several studies sustain the paradigm that uPAR conveys signals by interacting with members of the integrin family (Wei et al., 1996), chemotactic receptors


The Journal of Cell Biology, Vol. 179, No. 5, December 3, 2007 1067–1082
http://www.jcb.org/cgi/doi/10.1083/jcb.200702151

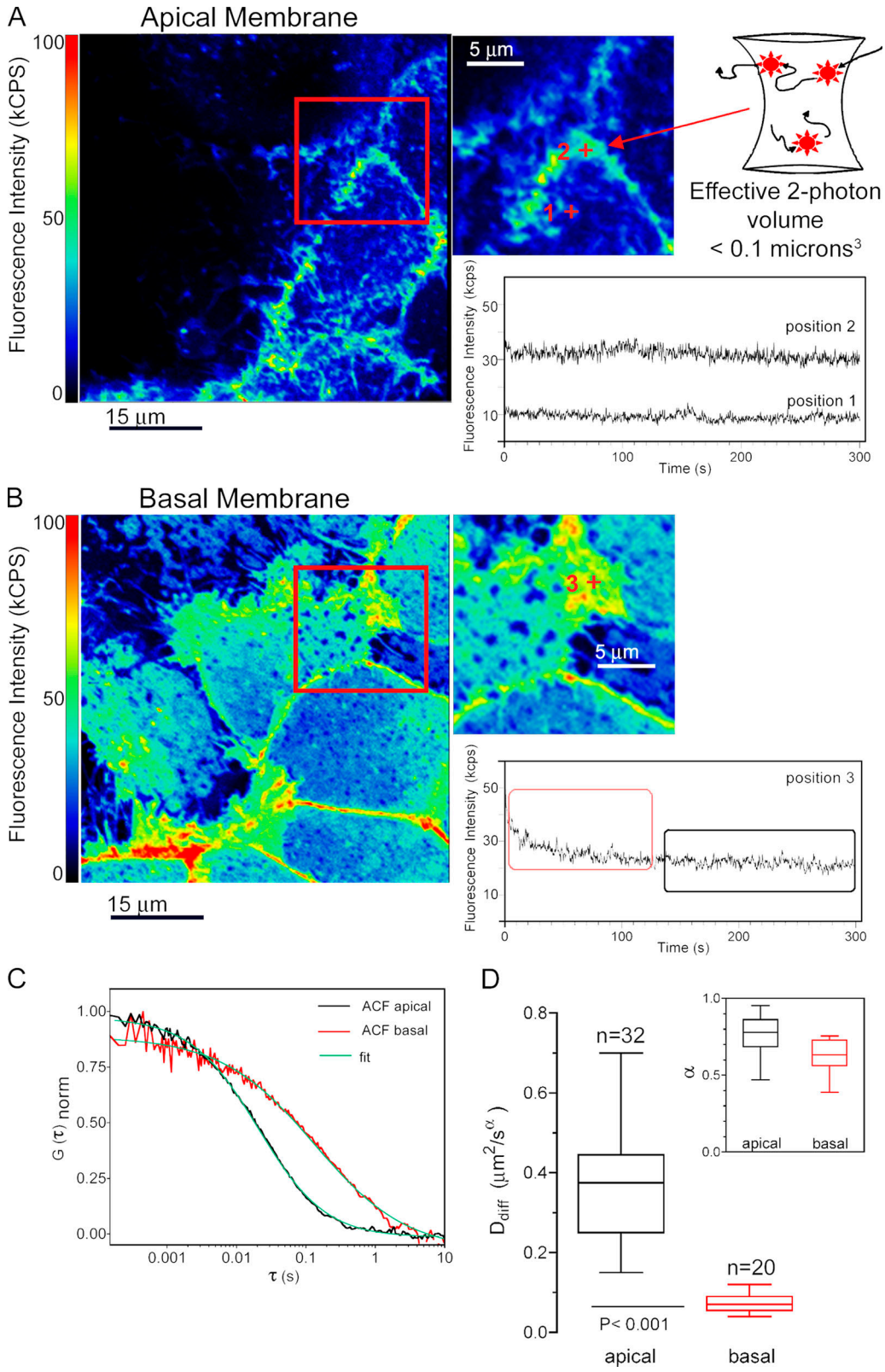


Figure 1. **Distribution and diffusion of cell surface uPAR-G in serum-plated HEK293 cells.** (A, left) Distribution of uPAR-G in apical membranes of live HEK293 cells. The magnified image of the boxed area shows two regions (positions 1 and 2) in which fluorescence intensity traces were acquired (bottom right). The scheme (top right) illustrates the typical two-photon volume selected for FCS measurements. (B, left) Distribution of uPAR-G in the basal membranes of the cells shown in A. The magnified image of the boxed area illustrates the region (position 3) in which the third FCS measurement of this example was taken. The trace acquired in position 3 (bottom right) shows an initial photobleaching (red rectangle subset). The diffusion coefficient of the residual mobile receptors was derived from the data at plateau (black rectangle subset). (C) Normalized autocorrelation functions (ACFs) derived from the fluorescence intensity traces acquired in position 2 in A and in position 3 in B. Green lines, curves fitted according to Eq. 1 (Fig. S2, available at http://www.jcb.org/cgi/content/full/jcb.200702151/DC1). (D) Diffusion coefficients and anomality coefficients ($\alpha$; inset) of uPAR-G in apical and basal membranes.

(Resnati et al., 2002), tyrosine kinase receptors such as the epidermal growth factor receptor (Liu et al., 2002), and proteins present in the extracellular matrix, including vitronectin (Vn; Wei et al., 1994; Kjoller, 2002; Madsen et al., 2007). In a previous study, we suggested that dimerization regulates the biological activity of uPAR by determining differential ligand binding and lipid raft partitioning (Cunningham et al., 2003). Detergent-resistant membrane fractions were enriched in uPAR dimers and coincided with higher Vn-binding activity (Cunningham et al., 2003). We have recently demonstrated that direct uPAR–Vn interaction is required and sufficient to initiate downstream changes leading to cell migration and signal transduction (Madsen et al., 2007). Nevertheless, the existence, distribution, and regulation of uPAR monomers and dimers in living cells have not yet been documented.

In this study, we have generated HEK293 cells expressing functional chimeras between uPAR and the monomeric EGFP (termed uPAR-G; Zacharias et al., 2002). We also generated HEK293 cells coexpressing uPAR-G and the chimera of the red (monomeric RFP1 [mRFP1]) variant (termed uPAR-R; Campbell et al., 2002). The dynamics of uPAR at the cell surface was studied by fluorescence correlation spectroscopy (FCS) using a subcloned cell population with homogeneously low expression of the green uPAR chimera. At the same time, we studied by Förster resonance energy transfer (FRET) the dimerization of the receptor in a pool of HEK293 cells cotransfected with the green and red chimeras of uPAR. FRET efficiency in these cells was robustly derived also in the presence of a relevant cell autofluorescence using the innovative phasor fluorescence lifetime imaging microscopy (FLIM; Digman et al., 2007). Our results demonstrate that membrane distribution, dynamics, and uPAR monomer–dimer exchange are determined by the interaction with Vn in the extracellular matrix. Our data also reveal that internalization and recycling mediated by the uPA–plasminogen activator inhibitor type 1 (PAI1) complex, a physiological ligand of uPAR, result in the disappearance of uPAR dimers from the cell surface by a reversible mechanism. Our data demonstrate that biologically relevant protein–protein interactions are major determinants of the dimerization and membrane dynamics of uPAR.

## Results

### Extracellular matrix Vn determines localization, association, and lateral diffusion of uPAR at the cell membrane

uPAR-G was constructed by inserting the sequence encoding the fluorescent proteins between the third domain of uPAR and the GPI-anchoring sequence at a position where we had previously epitope tagged uPAR without disrupting receptor function (Cunningham et al., 2003). The fluorescent chimera was stably transfected in the HEK293 cell line, as these cells do not express wild-type (wt) uPAR and do not secrete uPA. When expressed in HEK293 (termed HEK293/G), the chimera retains all of the tested biological activities of untagged wt-uPAR. uPAR-G is correctly GPI anchored, sorted to the cell surface, and partitions partially to detergent-resistant membrane similarly to untagged uPAR (Fig. S1 A, available at http://www.jcb.org/cgi/content/full/jcb.200702151/DC1). At the functional level, uPAR-G binds uPA with about twofold higher affinity than wt-uPAR (Fig. S1 B). This difference is negligible, as numerous affinities for uPA have been reported in a broad range (0.1–10 nM). The affinity for uPA is inversely proportional to the expression level (i.e., the higher the number of receptors, the lower the affinity; Picone et al., 1989). This may possibly explain the difference in affinity between wt-uPAR and uPAR-G. In our experiments, in fact, the saturating concentration of uPA was five times higher for wt-uPAR than for uPAR-G (Fig. S1 B). The relatively small difference in affinity for uPA is not likely to be of relevance in this study, as most of the experiments are conducted in the absence of uPA. The correct functioning of uPAR-G was also confirmed by the fact that it promotes pericellular plasminogen activation (Fig. S1 C) and supports uPAR-dependent cell adhesion to Vn (Fig. S1 D). Conventional fluorescence microscopy showed that uPAR-G localizes on the plasma membrane in lamellipodia, filopodia, and in intracellular vesicles and that it is heterogeneously distributed at the basal membrane, where it is recruited in intense patches (Fig. S1 E).

Having established the correct functionality of the receptor chimeras, we applied two-photon FCS for investigating the dynamics of uPAR-G at the apical and basal cell membranes. To select the best conditions for FCS and introduce only minimal perturbation into the system, we first undertook an extensive subcloning of the stable transfected HEK293/G pool and selected a cell clone with a homogenously low uPAR-G expression. The diffusion of one uPAR-G molecule in and out of a small volume defined by two-photon excitation (Fig. 1 A, top right scheme) gives rise to fluctuation of the fluorescence intensity from which diffusion coefficients can be derived by FCS analysis. To acquire fluorescence intensity traces, HEK293/G cells were first imaged in apical or basal planes (Fig. 1, A and B; left), and then the beam was positioned in specific regions (Fig. 1, A and B; indicated by +) on each plane (examples are given in Fig. 1, A and B; positions 1–3 in magnified areas), and intensity was recorded (Fig. 1, A and B; right). In the majority of the scanned submembrane regions of apical sections, the average intensity was constant during acquisition and in spots of different receptor density (Fig. 1 A, right; compare position 1 with position 2). In contrast, the fluorescence traces acquired in the bright regions of the basal membrane showed a decay of intensity as a result of photobleaching (Fig. 1 B, right; position 3). Photobleaching was observed only in basal planes and was not complete, suggesting that only a fraction of receptors was immobile during the acquisition of the fluorescence signal. 40–50% of uPAR-G molecules at the basal side of the cells photobleached, as estimated from the difference between the mean photon counts in the first 50 μs

Box-whisker plots show minimum, 25% percentile, median, 75% percentile, and maximum values. Three to four ACFs per cell were analyzed. The number of independent experiments (*n*) and statistical significance are indicated. Cells were seeded in serum-containing medium at 37°C, and fluorescence images and FCS measurements were recorded at 27°C 24–48 h later. kcps, kilocounts per second.

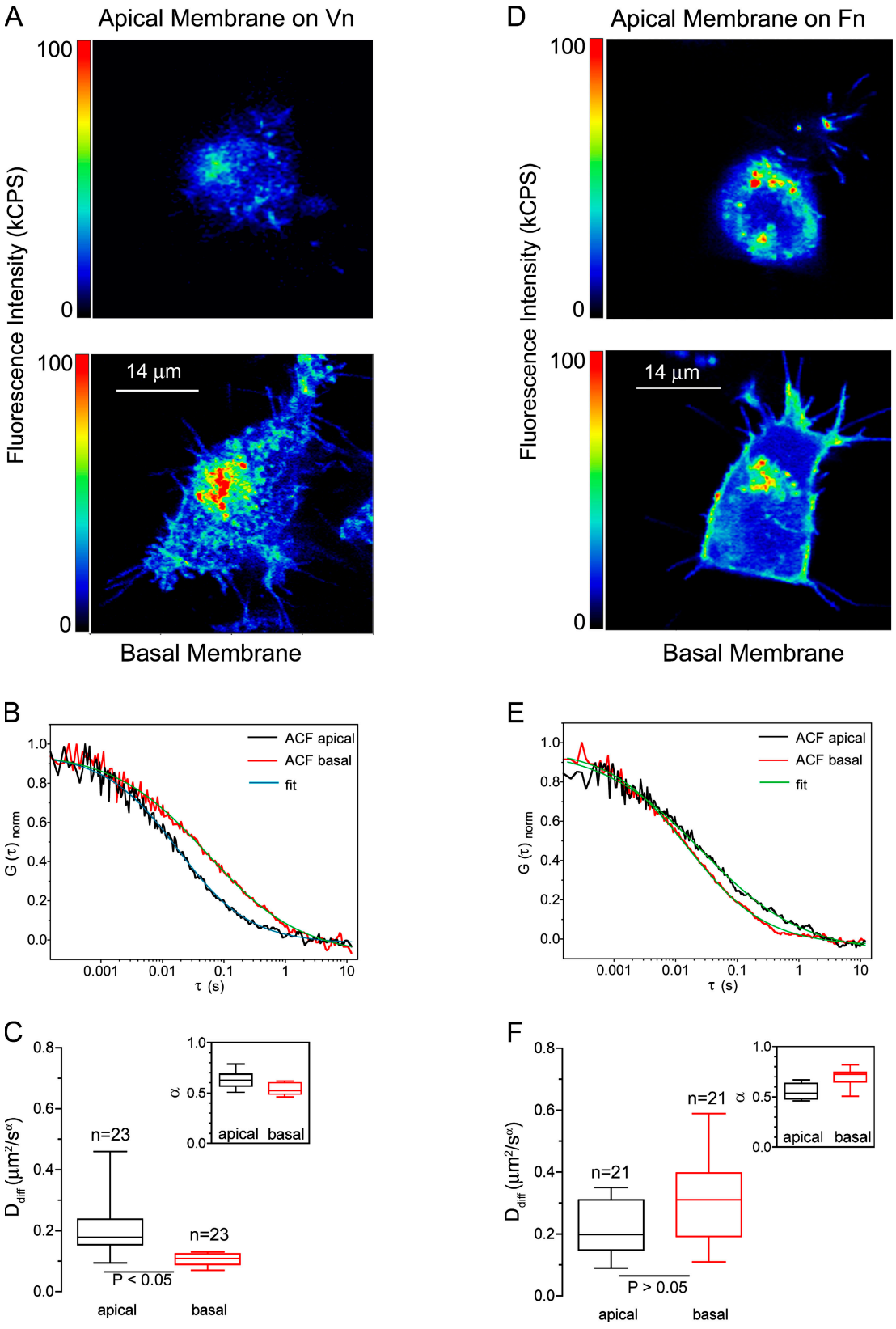


Figure 2. **Distribution and diffusion of cell surface uPAR-G in HEK293 cells adhered to Vn or Fn matrices.** (A and D) Distribution of uPAR-G in apical and basal membranes of HEK293 cells seeded on Vn (A) and Fn (D) matrices. (B and E) Representative normalized autocorrelation functions (ACFs) in one apical and one basal region are shown in B for cells on Vn and in E on Fn matrices. Green lines, curves fitted according to Eq. 1 (Fig. S2, available at http://www.jcb.org/cgi/content/full/jcb.200702151/DC1). (C and F) Diffusion coefficients and anomality coefficients (α; inset) of uPAR-G in apical and basal membranes are shown in C for cells on Vn and in F on Fn matrices. Box-whisker plots show minimum, 25% percentile, median, 75% percentile, and maximum values. Three to four ACFs per cell were analyzed. The number of independent experiments (*n*) and statistical significance are indicated. Cells were

after shutter opening and the mean of the photon counts at plateau. We used the unbleached portion of the fluorescence intensity trace to analyze the diffusion of the residual mobile uPAR-G fraction in these regions (Fig. 1 B, right; black marked subset).

The diffusion of uPAR-G at the cell apical or basal membrane was well described by the anomalous diffusion model, as shown by the fittings of the autocorrelation functions (ACFs) in Fig. 1 C (Schwille et al., 1999; Weiss et al., 2003; Banks and Fradin, 2005). The unacceptable results obtained with Brownian single or two-component models are discussed in Fig. S2 (available at http://www.jcb.org/cgi/content/full/jcb.200702151/DC1). The diffusion and the $\alpha$ (anomality) coefficients are summarized in Fig. 1 (D and inset). The mobile fraction at the basal membrane is slowed down, showing diffusion coefficients that were lower than those measured in the apical region of the cell membrane (Fig. 1 D) and suggesting that uPAR-G is involved in more stable interactions with the extracellular matrix or with other membrane proteins in tight contact with the matrix.

We recently documented that a direct interaction between uPAR on the cell surface and Vn in the matrix is crucial for the biological activities of the receptor in HEK293 cells (Madsen et al., 2007). To address the possibility that a direct interaction with matrix Vn could be responsible for the asymmetric distribution of diffusion coefficients between the basal and apical membranes, we next examined the diffusion of uPAR-G after seeding the cells on purified Vn or fibronectin (Fn; Fig. 2). The distribution of uPAR-G in the cell membrane is different on the two substrates. On Vn, uPAR-G was asymmetrically distributed and accumulated in patches at the basal membrane (Fig. 2 A, bottom). As for cells plated in serum-containing medium on Vn coating, ACFs taken in basal and apical membrane regions were fitted with the anomalous diffusion model (Fig. 2 B). At the basal membrane, uPAR-G photobleached as on serum (not depicted), and the residual mobile fraction had lower diffusion coefficients and smaller $\alpha$ values (Fig. 2, C and inset) in comparison with the apical membrane. In contrast, when cells were plated on Fn, uPAR-G did not accumulate into bright structures at the basal side (Fig. 2 D, bottom) and did not photobleach (not depicted). The ACFs were still anomalous (Fig. 2 E), but the diffusion coefficients were not significantly different in apical and basal membranes, indicating that uPAR-G was diffusing similarly on the two membrane sides. The diffusion coefficients of uPAR-G on Fn matrices did not differ from those measured in apical sides of cells seeded on Vn matrices (Fig. 2, F and inset; and see Table S1 for ANOVA analysis, available at http://www.jcb.org/cgi/content/full/jcb.200702151/DC1). For uPAR-G on both Fn and Vn matrices, the lower diffusion coefficients were associated with smaller $\alpha$ values and, therefore, with more confined diffusion (Fig. 2, C, F, and insets). However, only in cells seeded on Vn matrices was the diffusion of uPAR-G significantly different in apical versus basal membrane (Table S1). The mobility of the receptor on Vn matrices reproduced that observed in cells seeded in serum-rich medium (which is indeed rich in Vn), although the absolute values of the diffusion coefficients in serum and on Vn matrices are not strictly comparable because of the different cell culture conditions. In fact, for the experiments on Vn (or Fn) matrices, cells were maintained in medium without serum for only 2–4 h before measurement and were not at subconfluency (as for serum after 24–48 h). These results demonstrate that Vn is responsible for the recruitment of uPAR-G to the basal membrane and for the engagement of uPAR in the cell adhesion process.

### uPAR dimers are selectively recruited to Vn matrices

Because the Vn binding–competent form of uPAR has been suggested to be a dimer (Sidenius et al., 2002; Cunningham et al., 2003), we next analyzed the distribution of uPAR monomers and dimers on the cell surface by FRET on a pool of HEK293 cells coexpressing uPAR-G as the donor and the corresponding chimera carrying the mRFP1, uPAR-R, as the acceptor. These cells (termed HEK293/GR) were stably transfected but not subcloned and had a heterogeneous expression of the green and red uPAR chimeras (Fig. S3, available at http://www.jcb.org/cgi/content/full/jcb.200702151/DC1).

We analyzed FRET after the decrease of the donor fluorescence lifetime using a novel approach to FLIM (Digman et al., 2007). Several reasons prompted us to improve the analytical approach for deriving FRET efficiencies by FLIM in living cells: (1) EGFP lifetime is multiexponential (Suhling et al., 2002); (2) the contribution of cell autofluorescence to the signal tends to decrease the lifetime, and it could be confused with the occurrence of FRET; (3) the heterogeneity of donor-G and acceptor-R expression in pools of transfected cells (Fig. S3); and (4) the need to examine a large number of cells. Given these issues, we were not satisfied by the reproducibility, accuracy, and/or easiness of more standard FRET methods, steady-state or time-correlated single-photon counting (TCSPC) FLIM.

To overcome these obstacles, we took advantage of the well-known sensitivity of TCSPC-FLIM methods, avoiding the approximate analysis of multiexponential decays, and developed the phasor-FLIM approach (Digman et al., 2007), which is illustrated in Fig. 3. TCSPC-FLIM data were transformed in the phasor representation (see Materials and methods). In this representation, the fluorescence decay in each pixel of the image gives a point in the phasor plot. Only single exponential decays fall on the universal circle (Fig. 3 A, position a). If the decay at one pixel is a convolution of lifetimes, as a result of multiple species contributing to the fluorescence intensity in that pixel, the phasor falls inside the universal circle, and it is simply the algebraic sum of phasors from each component (Fig. 3 A, position b; Gratton et al., 1984; Clayton et al., 2004; Redford and Clegg, 2005). Several subcloned HEK293/G as well as untransfected HEK293 cells were imaged in TCSPC mode and represented in the phasor plot. The phasor distributions of three of these samples are shown in Fig. 3 B as contour plots. In Fig. 3 B,

seeded in serum-free medium on dishes coated with 2.5 μg/ml Vn or 10 μg/ml Fn and were allowed to recover for 2–4 h at 37°C before the recording of fluorescence images and FCS at 27°C. kcps, kilocounts per second.

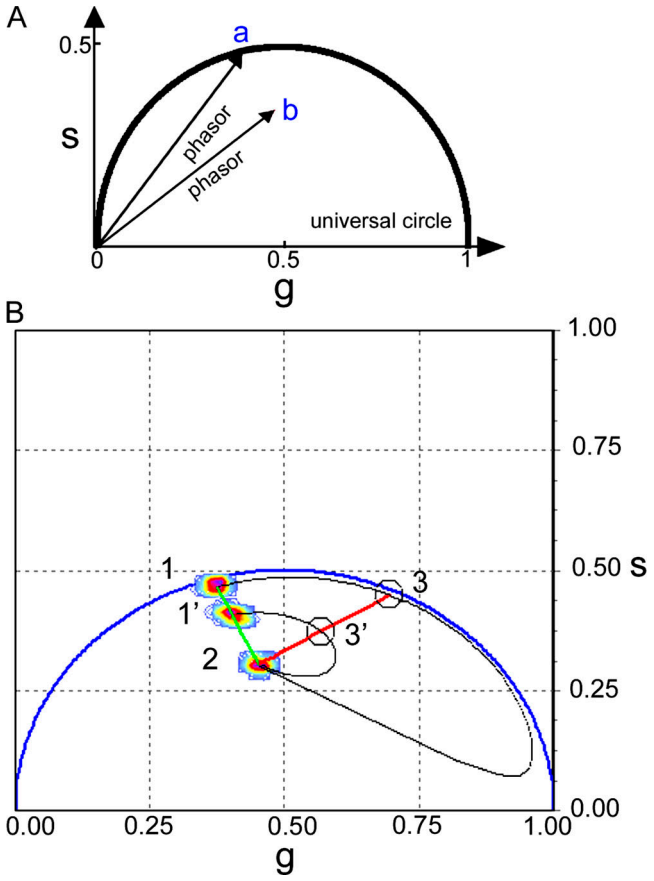


Figure 3. **Fluorescence lifetime analysis of HEK293/G cells by Phasor-FLIM.** (A) The universal circle of the phasor representation showing a single lifetime phasor (position a) and a phasor arising from a complex lifetime decay (position b; see Materials and methods for the phasor transformation of fluorescence lifetime decays). (B) Representative phasor distributions. TCSPC-transformed decay data at each pixel are shown in contour plots for the basal membranes of two HEK293/G cells at high (position 1) and low (position 1′) uPAR-G expression. The basal membrane of an untransfected HEK293 cell (cell autofluorescence) is represented by the contour plot in position 2. HEK293/R cells behave as untransfected HEK293 under identical experimental conditions (not depicted). The green line is the trajectory joining the mean values of the phasor distributions in HEK293/G at different contributions of cell autofluorescence. The black lines are the calculated FRET trajectories describing all possible positions of the uPAR-G phasors in the presence of quenching as a result of FRET for the basal membranes imaged in positions 1 and 1′ having a cell autofluorescence contribution of 1% and 37%, respectively. The FRET trajectories are computed using the phasor of the donor in the absence of FRET (positions 1 and 1′) and the phasor of the background (position 2), which were determined independently on untransfected cells, and applying the classic definition of FRET efficiency, $[1 - (\tau_{donor\text{-}acceptor})/\tau_{donor}]$, to determine the phasor corresponding to the quenched donor. All possible phasors that are quenched with different FRET efficiencies (from 0 to 100%) describe a curved trajectory (black line) in the phasor plot. The experimental position of the phasor of a given sample along the trajectory determines the amount of quenching and, therefore, the FRET efficiency. The contributions of the background and of the donor without acceptor is evaluated using the rule of the linear combination with the background phasor (which was determined independently) and the donor unquenched (which was also determined independently). As an example, the circles 3 and 3′ mark the positions corresponding to the phasor distributions 1 and 1′ with 50% FRET quenching. Thus, the red line marks the position of uPAR-G phasors at 50% FRET and having all possible cell autofluorescence contributions (0–100%).

position 1 and 1′ identify the basal membrane of two HEK293/G cells at high and low uPAR-G expression, respectively. Position 2 in Fig. 3 B localizes the phasor distribution of the cell autofluorescence, which was measured in untransfected HEK293 under identical experimental conditions. The experimentally derived green line in Fig. 3 B represents the mean phasor distribution for unquenched donors with different contributions of cell autofluorescence.

Once we know the phasor of the unquenched donor and of the cell autofluorescence, we can calculate the FRET trajectory in the phasor plot (Fig. 3 B, black lines; Digman et al., 2007). This trajectory describes the possible positions of the donor phasor in the presence of FRET. Along the trajectory, we can identify the points corresponding to the Förster distance for this pair of fluorescent proteins (Patterson et al., 2000), giving the 50% FRET efficiency at different cell autofluorescence contributions (Fig. 3 B, red line; positions 3 and 3′ are two examples). In all of our experiments, phasors resulting from any combination of unquenched uPAR-G, FRET-quenched uPAR-G, and cell autofluorescence fall within the area delimited by the green and red lines in the phasor plot (Fig. 3 B).

Fig. 4 (A and B) illustrates a reference experiment on a HEK293/G cell. For each membrane section, the fluorescence intensity image, the phasor plot, and the FLIM image (Fig. 4, A and B; pink mask) are shown. In both phasor plots of Fig. 4 (A and B), the black circle includes the area in which the majority of the donor phasors (>95%) were found. The radius of this circle, which was obtained from analysis of the phasor distribution in 40 donor cells (unpublished data), determines the confidence limit for FRET analysis in our cell system. This limit is equivalent to 8% FRET efficiency (i.e., FRET efficiencies below 8% are not significant). We used a circle with identical radius for analyzing the phasor distributions in HEK293/GR cells. A representative FRET experiment is illustrated in Fig. 4 (C and D). In this case, the phasor distribution in both basal and apical membranes has moved apart from the green line, indicating that some donors are quenched by FRET (Fig. 4, A and B; compare the phasor distributions in the control HEK293/G cell). In the basal membrane, 82% of the pixels in the image are within the range of 8–24% FRET (Fig. 4 C, FLIM; top), whereas only 8% of pixels at the border of the basal membrane show negligible FRET (Fig. 4 C, FLIM; bottom). In the apical membrane, we observed the reverse. The majority of pixels (70%) do no show significant FRET (Fig. 4 D, FLIM; bottom), whereas only 30% of pixels are picked within the range of 8–24% FRET (Fig. 4 D, FLIM; top).

The same results were obtained when HEK293/GR cells were seeded on a Vn matrix under serum-free conditions (Fig. 5, A and B). FRET is mainly measured at the basal membrane (Fig. 5 A, FLIM; top), whereas a large fraction of pixels at the apical membrane shows unquenched donor phasors (Fig. 5 B, FLIM; bottom). Conversely, when HEK293/GR cells were plated on Fn coating, FRET was minimal in both basal (Fig. 5 C) and apical (Fig. 5 D) membranes.

We have analyzed a relevant number of cells and, for each basal and apical image, evaluated a mean FRET efficiency. In Fig. 6, the results from at least 26 cells in each serum condition,

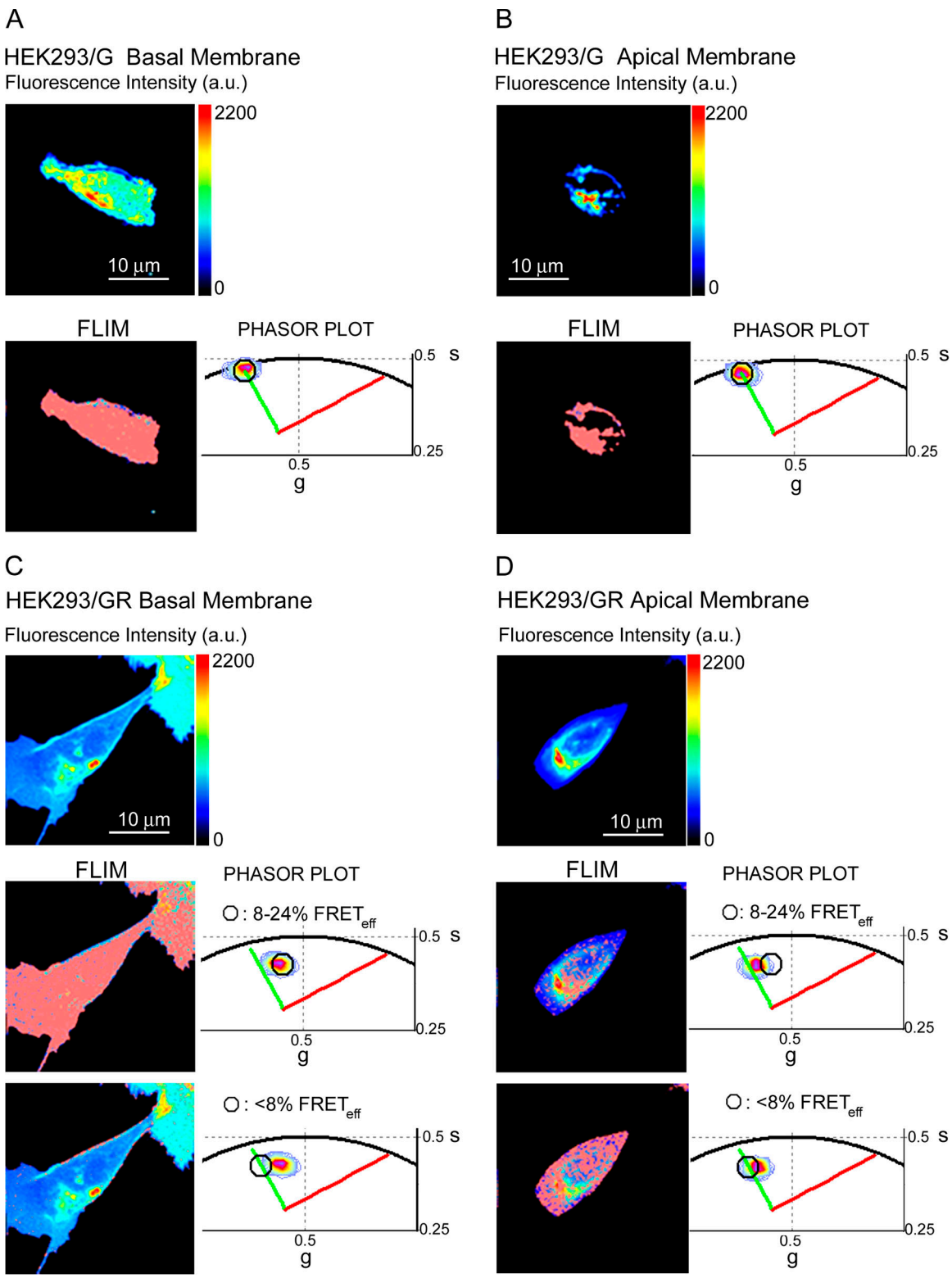


Figure 4. **Distribution of uPAR-GR dimers at the apical and basal membranes of HEK293/GR cells seeded in the presence of serum.** (A and B) A representative phasor-FLIM experiment on a HEK293/G cell imaged at the basal (A) and apical (B) membranes shows the fluorescence intensity image, the phasor plot, and localization in the FLIM image (pink masks) of the pixels comprised in the selected area (black circles) of the phasor plot. The black circles in this example select 98% of the total pixels of the image. The fluorescence lifetime of uPAR-G does not depend on its local concentration, as pixels with high and low intensity are included in the phasor selection. (C and D) The parallel experiment on a HEK293/GR cell is reported in C for the basal and D for the apical membranes. Two phasor subsets are shown in the phasor plots, and the correspondent pixels are localized in the FLIM images: pixels included in the 8–24% (top) and <8% (bottom) FRET efficiency ranges. Cells were seeded in serum-rich medium and kept at 37°C and 5% $CO_2$ for 48 h. Fluorescence images and FLIM measurements were performed at 27°C.

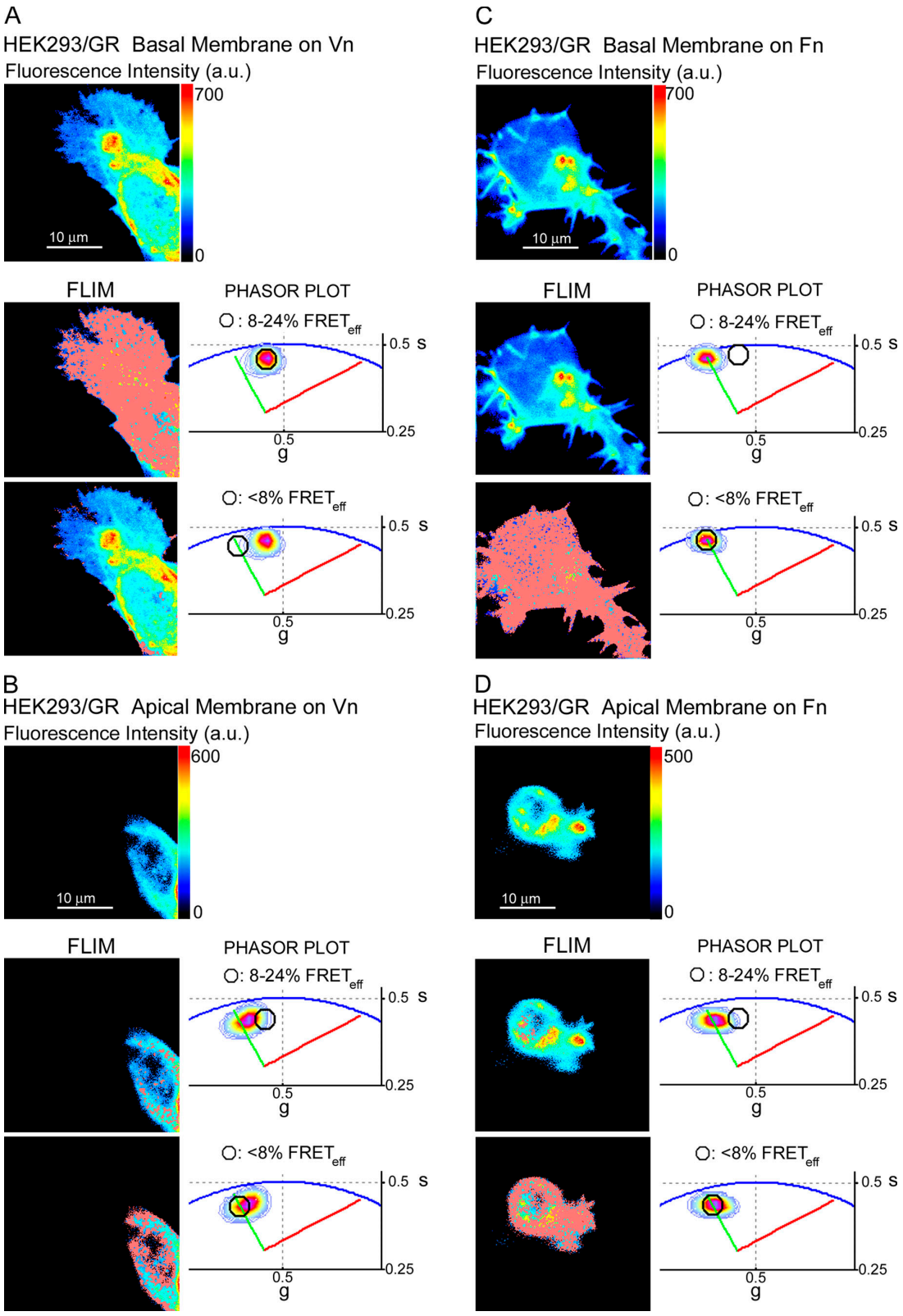


Figure 5. **Distribution of uPAR-GR dimers at the apical and basal membranes of HEK293/GR cells seeded on Vn or Fn matrices.** (A–D) Representative phasor-FLIM experiments on HEK293/GR cells on Vn matrix (A and B) and on Fn matrix (C and D). Each panel shows the fluorescence intensity image and two phasor subsets (black circles in the phasor plots). The correspondent FLIM images illustrate the localization of the pixels selected in each subset: 8–24% (top) and <8% (bottom) FRET efficiency ranges. Cells were seeded in serum-free medium on dishes coated with 2.5 µg/ml Vn or 10 µg/ml Fn and allowed to recover for 2–4 h at 37°C before recording fluorescence images and FLIM at 27°C.

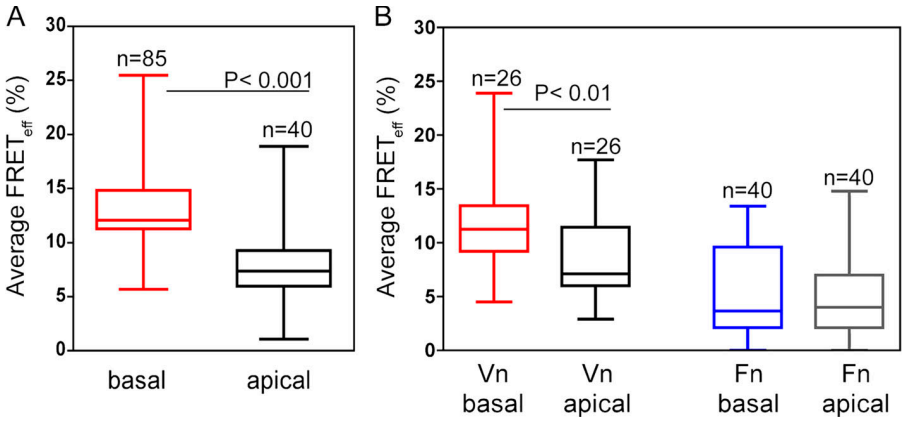


Figure 6. **Statistical analysis of mean FRET efficiencies in HEK293/GR cells.** (A and B) Mean FRET efficiencies derived from the phasor distributions acquired in basal and apical membranes of HEK293/GR cells grown in serum-containing medium (A) or seeded on purified Vn or Fn (B) matrices. The box-whisker plots show minimum, 25% percentile, median, 75% percentile, and maximum values. The number (*n*) of independent experiments is indicated. Statistical significance is either indicated in the plot or reported in Table S1.

Vn and Fn, are reported (the number of cells/experimental condition is specified in the figure). The mean FRET efficiency was obtained as the mean FRET efficiency in each phasor plot of each imaged membrane side. Data from all experiments performed under the three conditions (on serum coating and on purified Vn as well as Fn matrices) are summarized in the box-whisker plots of Fig. 6. Despite mean FRET spreads in a wide range, as a result of the different expression levels of uPAR-G and uPAR-R (Fig. S3) in the cotransfected HEK293 pool, the analysis clearly confirms that FRET is relevant in basal membranes of HEK293/GR cells either grown on serum coating (Fig. 6 A) or seeded on purified Vn (Fig. 6 B). Furthermore, the analysis also confirms that in apical membranes, FRET is significantly lower (Fig. 6, A and B; and Table S1). In contrast, FRET observed in cells seeded on purified Fn was overall lower and similar in basal and apical membranes (Fig. 6 B and Table S1). Collectively, these data demonstrate that the distribution of cell surface uPAR monomers and dimers under steady-state conditions is determined by the presence of Vn in the extracellular matrix and that the dimeric receptor is the molecular form of uPAR predominantly recruited to matrix Vn.

### Binding of uPA–PAI1, endocytosis, and recycling affect dimerization and dynamics of uPAR

When cultured under serum-containing conditions, uPAR-expressing HEK293 cells are highly motile, and this motility requires a direct uPAR–Vn interaction (Madsen et al., 2007). Because cell motility entails coordinated and localized attachment and detachment from the substratum, we speculated that cellular processes such as receptor endocytosis and recycling could provide the cell with a mechanism to regulate the dynamics of uPAR dimerization and, thus, cell adhesion. To address this possibility directly, we next analyzed the effects of saturating concentrations of uPA–PAI1 (a catalytically inactive protease–serpin complex) on uPAR dimerization and dynamics. PAI1 exerts its activity through a covalent binding and inactivation of uPA. After binding to uPAR, the uPA–PAI1 complex is internalized by a mechanism that involves one or more members of the low-density lipoprotein receptor family, including LRP1 (Cubellis et al., 1990; Nykjaer et al., 1992). After internalization, the uPA–PAI1 complex is degraded in lysosomes, and uPAR recycles to the cell surface (Conese and Blasi, 1995; Nykjaer et al., 1997). To initiate internalization of the receptor, we incubated the cells on serum coating at 37°C for 30 min in the presence of uPA–PAI1 and subsequently acquired fluorescence intensity images, fluctuation traces, and FLIM at 27°C to slow down internalization and recycling during data acquisition. Under these conditions, the internalization of the complex uPAR/uPA–PAI1 is incomplete, allowing for the analysis of residual cell surface uPAR (Fig. 7, A and B; top). Incubation of cells with uPA–PAI1 resulted in the loss of FRET in both basal and apical membranes (Fig. 7, A and B; FLIM and phasor plots) in the majority of the cells (Fig. 7 C). Control experiments documented that donor phasors in HEK293/G cells were not affected by uPA–PAI1 (unpublished data). Thus, the loss of FRET demonstrates that uPAR-GR dimers are disassembled upon uPA–PAI1 binding.

To further substantiate this finding, we performed photon-counting histogram (PCH) analysis of fluorescence intensity traces collected on apical membranes of HEK293/G cells exposed to uPA–PAI1. Combining PCH and FCS analyses, we could derive the brightness of the uPAR-G/uPA–PAI1 complexes in parallel to their diffusion coefficient (Fig. 8). At a single-molecule level, the brightness, which is the photon counts per second per molecule (cpsm), reports on the presence of homotypic uPAR-G assemblies that codiffuse in the membrane (Chen et al., 1999). In the presence of uPA–PAI1, the diffusing complex has only the brightness of uPAR-G monomers (Fig. 8 A), as it is comparable with that of free monomeric EGFP in solution (Fig. 8 A, inset). In the absence of uPA–PAI1 (Fig. 8 B), the brightness of uPAR-G indicated the presence of monomers and, in some cases, dimers, as it increased to twice the brightness of free EGFP (Fig. 8 A, inset). This result confirmed the aforementioned finding on HEK293/GR cells that the binding of uPA–PAI1 disassembles uPAR dimers. Additionally, as brightness values significantly >10,000 cpsm were only rarely found in any tested condition (with or without uPA–PAI1; Fig. 8, A and B), the data also confirm previous observations (Cunningham et al., 2003) excluding, or at least strongly limiting, the existence of uPAR assemblies larger than dimers diffusing as a whole in resting living cells.

We also analyzed by FCS the fluorescence fluctuation traces acquired in the presence of uPA–PAI1 (Fig. 8, C and D). Although diffusion in cell membranes cannot be directly related to

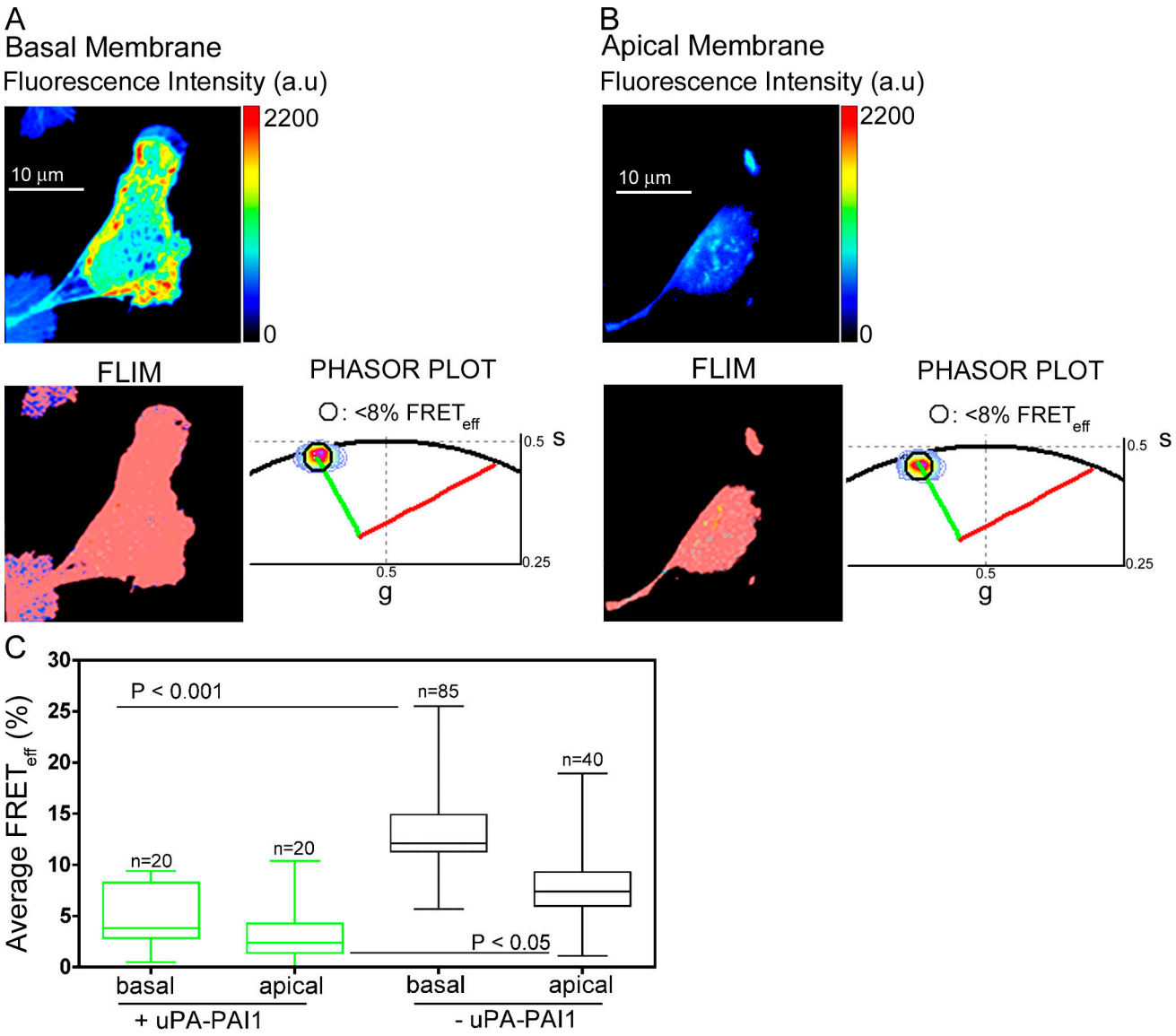


Figure 7. **Loss of uPAR-GR dimers in HEK293/GR cells exposed to uPA–PAI1.** (A and B) Representative phasor-FLIM experiment on a HEK293/GR cell, which was grown and maintained in serum-rich medium, exposed to 8 nM uPA–PAI1 for 30 min at 37°C and imaged at 27°C on the basal (A) and apical (B) membranes. Each panel shows the fluorescence intensity image and the phasor plot in which the black circles select phasor subsets of <8% FRET efficiency. The black circles in this example include 95% of pixels of the images. The correspondent FLIM panels show the localization of these pixels in the images (pink masks). (C) The mean FRET efficiency measured in HEK293/G exposed to uPA–PAI1 is reported. The box-whisker plots show minimum, 25% percentile, median, 75% percentile, and maximum values. The data in the absence of uPA–PAI1 are shown for comparison and are reproduced from Fig. 6 A. The number of independent measurements (*n*) and statistical significance are shown.

protein mass (Muller et al., 2003), the internalization complex induced by uPA–PAI1 has a molecular weight much larger than that of uPAR-G (Cubellis et al., 1990; Nykjaer et al., 1992), and its effect on the diffusion of the receptor was detected. The ACFs were fitted by the anomalous diffusion model (Fig. 8 C) and indicated that the binding of uPA–PAI1 slowed down the diffusion of uPAR-G in apical membranes (Fig. 8, D and inset). In the basal membrane, although intense patches were still observed (Fig. 7 A, top), cell adhesion was compromised to the point that we could not acquire fluorescence intensity traces in these regions.

The loss of uPAR dimers induced by uPA–PAI1 was reversed by washing the cells and allowing full recycling for 2 h at 37°C before imaging at 27°C (Fig. 9). After recycling, FRET was higher in basal (Fig. 9 A, FLIM and phasor plot) than in apical (Fig. 9 B, FLIM and phasor plot) membranes, and the reversibility of the effect was observed in the majority of the cells (Fig. 9 C). Collectively, these data demonstrate that the commitment to endocytosis induces an exchange between uPAR monomers and dimers at the cell surface, depleting the receptor dimers. The process is reversible, as the recycling of uPAR is sufficient for the dimers to reform and relocate to the cell matrix interface.

## Discussion

Monomeric and dimeric uPAR were shown to display different ligand-binding specificities and different resistance to detergent

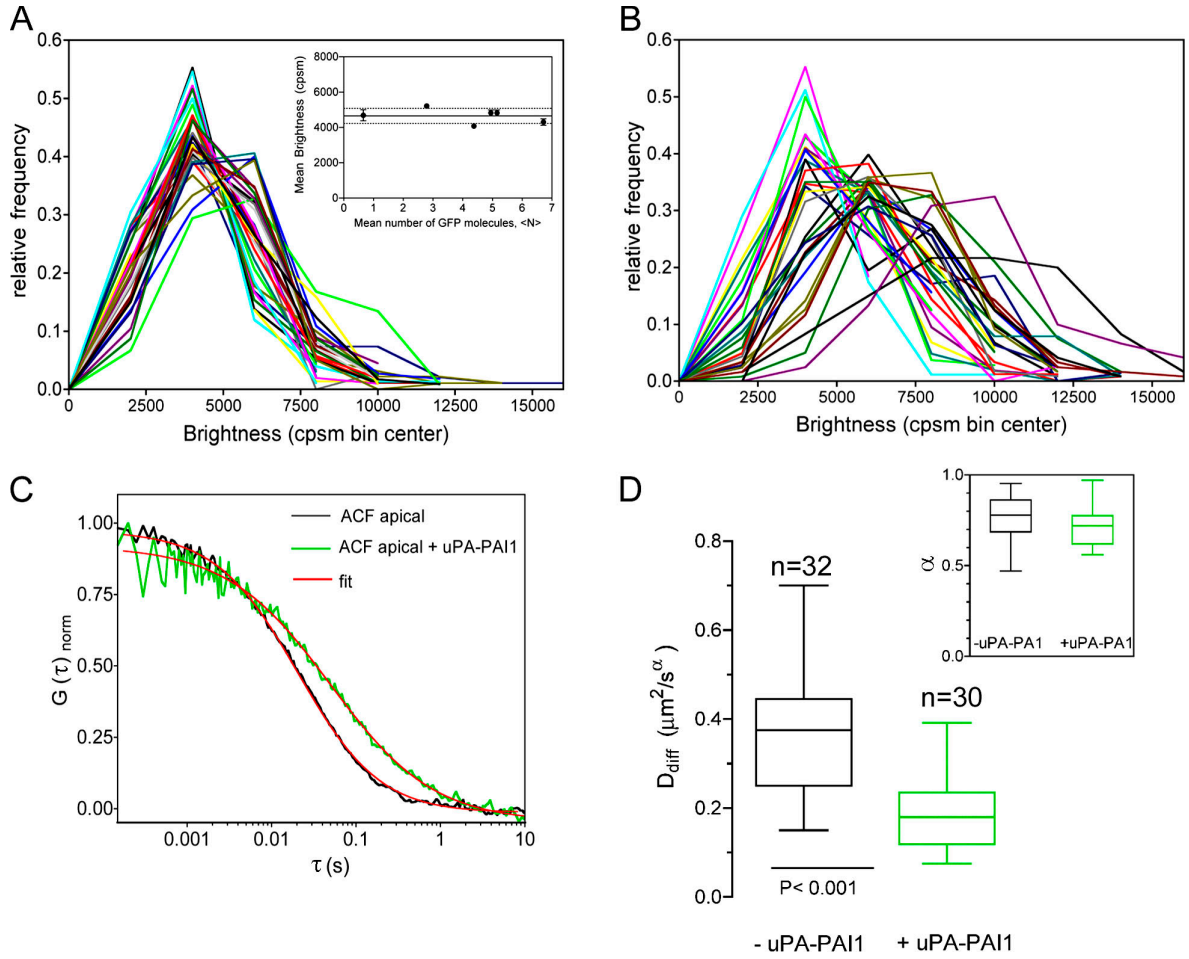


Figure 8. **Loss of uPAR-G dimers in HEK293/G cells exposed to uPA–PAI1 and diffusion of the uPAR-G/uPA–PAI1 complexes at the cell surface.** (A) Plot of the relative frequency of the brightness obtained by local PCH analysis in apical membranes of HEK293/G cells exposed to uPA–PAI1 as described in Fig. 7. Brightness was derived taking intervals of 2.5 s on the fluorescence fluctuation traces (see Materials and methods; Chen et al., 2002). Each curve is an independent measurement (i.e., a fluorescence intensity trace; $n = 30$). (inset) Mean brightness of monomeric EGFP in solution as a function of the concentration expressed as the mean number of molecules (Chen et al., 1999). Each EGFP solution was tested in triplicate. The mean brightness of monomeric EGFP in solution was 4,746 cpsm (minimum 4,077 cpsm, maximum 5,210 cpsm). (B) Plot of the relative frequency of brightness in the absence of uPA–PAI1. The brightness was determined as in A. Each curve is an independent measurement (i.e., a fluorescence intensity trace; $n = 32$). (C) Representative normalized autocorrelation functions (ACFs) in apical regions of HEK293/G cells before (black line) and after (green line) exposure to 8 nM uPA–PAI1 for 30 min at 37°C. Red lines, curves fitted according to Eq. 1 (Fig. S2, available at http://www.jcb.org/cgi/content/full/jcb.200702151/DC1). (D) Diffusion coefficients and anomality coefficients (α, inset) of uPAR-G in apical membranes of HEK293/G cells exposed to uPA–PAI1. Box-whisker plots indicate minimum, 25% percentile, median, 75% percentile, and maximum values. Three to four ACFs per cell were analyzed. The number of total measurements (*n*) and statistical significance are shown. The data from HEK293/G not exposed to uPA–PAI1 are shown for comparison and are reproduced from Fig. 1 D. Cells were grown and maintained in serum-rich medium and imaged at 27°C.

extraction, as detergent-resistant fractions were enriched of dimers and coincided with the higher Vn-binding activity (Cunningham et al., 2003). However, little is known about the regulation of dimerization as well as the membrane distribution of monomeric and dimeric forms of the receptor. We have previously proposed that the interaction between uPAR and other proteins in the membrane, apart from uPA, or segregation of uPAR in membrane microdomains could control dimerization (Cunningham et al., 2003). To address these issues in live cells, we have used biologically active fluorescent chimeras of the GPI-anchored uPAR and studied single-molecule dynamics and distribution of uPAR monomers and dimers on the cell surface.

We have applied two-photon FCS and FRET by phasor-FLIM in the presence of physiological ligands of uPAR in live cells without any artificial cross-linking or antibody-induced clustering with the intent of working at steady-state conditions (Kusumi and Suzuki, 2005). We analyzed the effect of uPAR binding to its extracellular matrix ligand Vn (present in high quantities in the serum-containing media used for cell culture; Madsen et al., 2007) as well as the effect of endocytosis and recycling induced by the extracellular uPA–PAI1 complex. Under these conditions, we systematically measured the diffusion properties of uPAR in multiple regions of the apical and basal cell membranes and the homotypic interactions of the receptor.

We found pronounced effects of these ligands on uPAR dynamics and dimerization. In the extracellular matrix, Vn affects the distribution of uPAR in the cell membrane and the compartmentalization of monomers and dimers of the receptor in apical and basal sides, as shown by fluorescence imaging and FRET analysis on live cells. When cells are seeded on Vn, uPAR

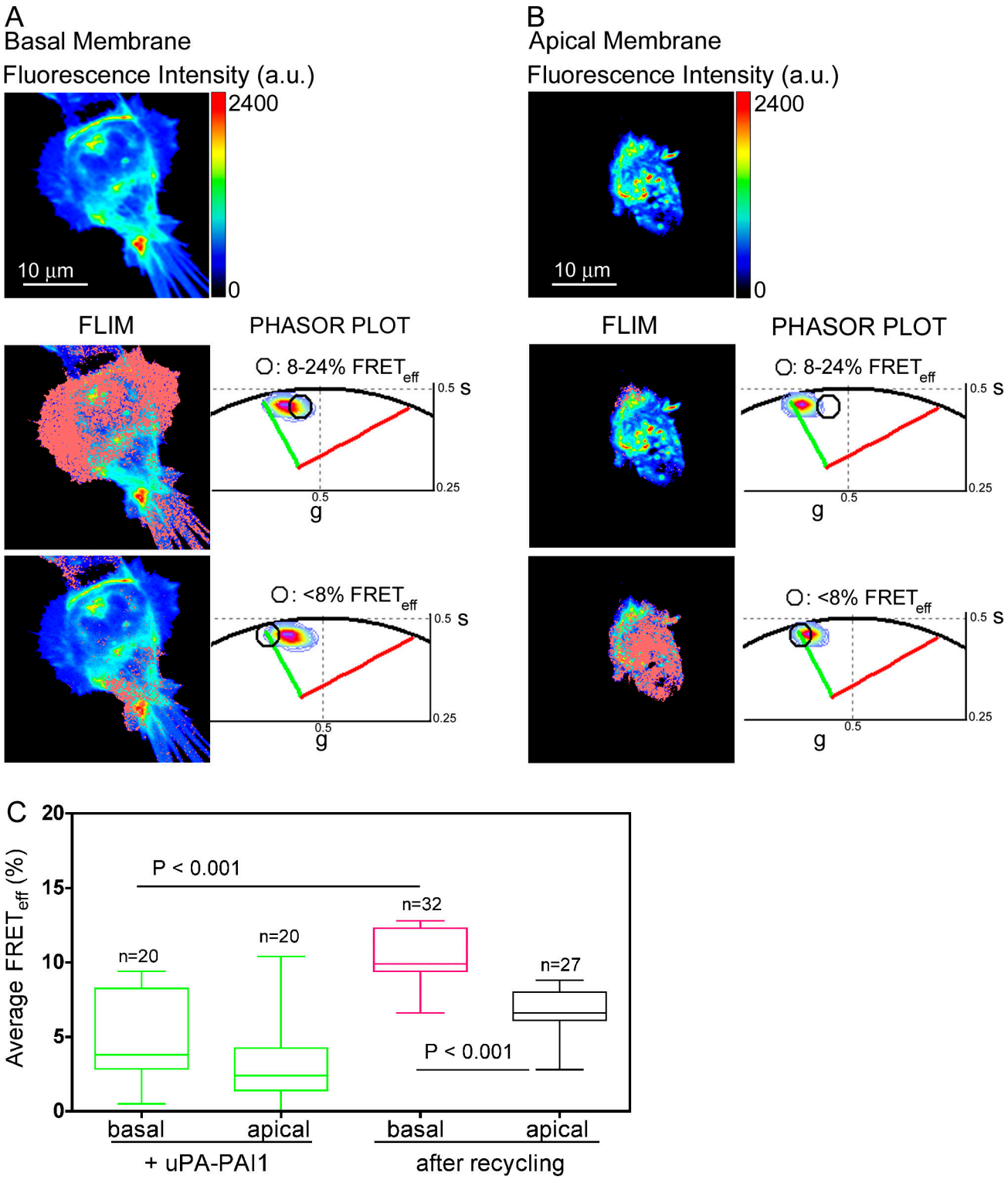


Figure 9 . **Recovery of uPAR-GR dimers in HEK293/GR cells after endocytosis and recycling.** (A and B) Representative phasor-FLIM experiment on the basal (A) and apical (B) membrane of a HEK293/GR cell grown on serum-coating exposed to uPA–PAI1 for 30 min and then left to recycle for 2 h at 37°C in fresh, serum-rich medium lacking uPA–PAI1 before imaging at 27°C. Each panel shows the fluorescence intensity image and two phasor subsets (black circles in the phasor plots). The correspondent FLIM images illustrate the localization of the pixels selected in each subset: 8–24% (top) and <8% (bottom) FRET efficiency. (C) The mean FRET efficiency measured in HEK293/G after recycling is reported. The box-whisker plots show minimum, 25% percentile, median, 75% percentile, and maximum values. The numbers (*n*) of independent measurements and statistical significance are indicated. The data in the presence of uPA–PAI1 (i.e., in the absence of recycling) are shown for comparison and are reproduced from Fig. 7 C.

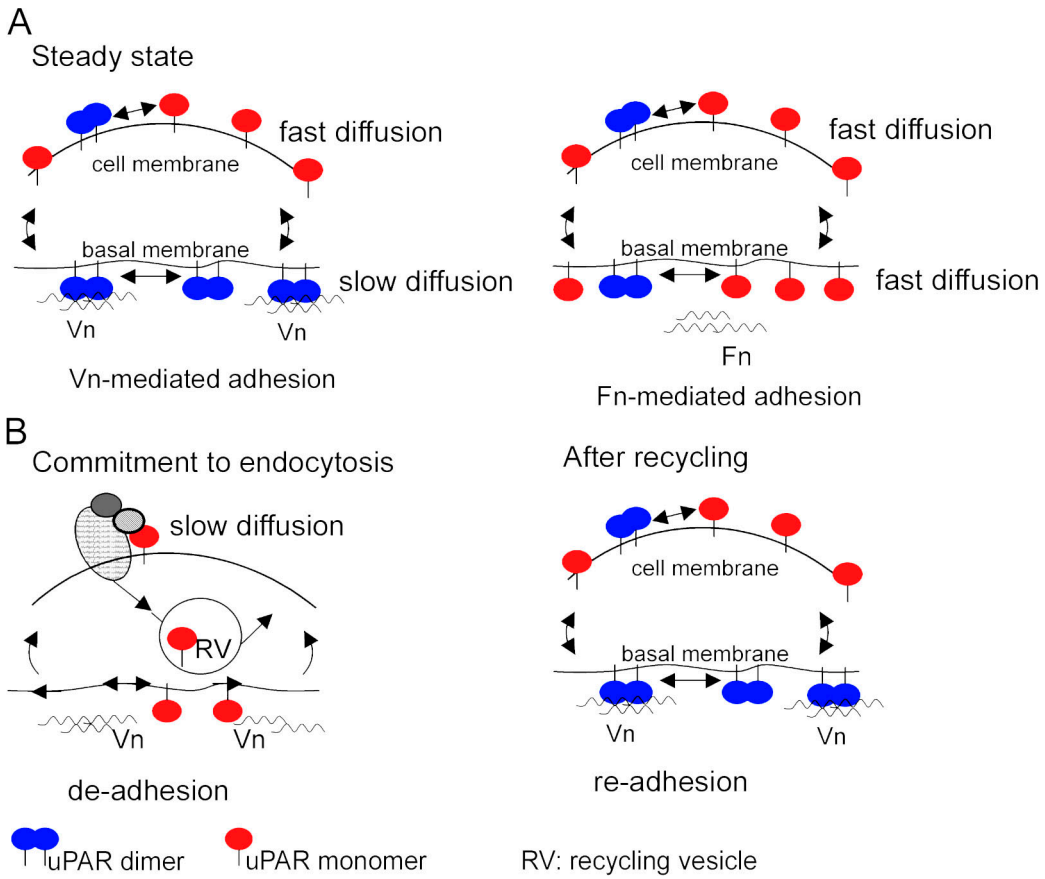


Figure 10. **uPAR monomer–dimer dynamics on the cell surface.** (A) At steady state, Vn in the extracellular matrix (left) recruits and stabilizes uPAR dimers in the basal membrane. uPAR dimers are the dominant form in the basal membrane. As a result of the interaction with Vn, 40–50% of uPAR is immobile, and the rest diffuses more slowly and more anomalously than in apical sides. Receptors not engaged in matrix contact (i.e., receptors in the apical membrane) are in equilibrium between dimeric and monomeric forms, the latter being the most prominent; both forms display fast diffusion in this membrane side. When cells are seeded on Fn (right), a different picture is observed: there is no polarized distribution of uPAR between the basal and apical membranes, dimers are generally rare, and fast, lateral diffusion is observed throughout the cell membrane. (B) Commitment to endocytosis (left) through uPA–PAI1, binding depletes dimeric uPAR from the cell surface and destabilizes adhesion to Vn. The monomerization induced by commitment to endocytosis is reversible, and recycling is followed by the de novo formation of uPAR dimers and reestablishes the firm adhesion (right).

is recruited to the basal membrane and distributed in bright patches at the cell matrix interface. The massive recruitment on matrix Vn clearly involves uPAR dimers, whereas only few dimers are found in the apical side of the cell. On Fn matrices, the receptor is found uniformly distributed at the membrane border and in filopodia, and dimers are rare in the basal membrane as in the apical membrane because negligible FRET is measured at the surface of cells seeded on these matrices. These data substantiate recent findings demonstrating that the biological activity of uPAR in cell adhesion and migration requires a direct interaction between uPAR and matrix Vn (Madsen et al., 2007) and confirm previous observations suggesting that Vn interacts preferentially with uPAR dimers (Cunningham et al., 2003).

We also observed a systematic difference in the dynamics of the receptor on different matrices by FCS analysis. On Vn, a fraction (40–50%) of uPAR was immobile (irreversibly photobleached) in the basal membrane, and the residual mobile fraction diffused more slowly than in apical regions. In contrast to the observations that uPAR associates with Fn integrins and regulates their activity (Wei et al., 1996, 2007; Chaurasia et al., 2006), we observed fast diffusion and no measurable bleaching of uPAR-G when the cells were seeded on Fn matrices, indicating that only a minor fraction of uPAR could be associated with integrins bound to Fn. The diffusion of uPAR is anomalous (i.e., not explained by a simple Brownian diffusion) not only in the basal membrane of cells adherent on Vn but also in all other analyzed conditions. Because of the complexity of the membrane morphology (membrane wrinkles) and cell movements, anomalous diffusion can arise as a pure geometrical effect even if the particle diffuses normally (Sbalzarini et al., 2005). The latter effect may account partly for the anomalous diffusion of uPAR. Nevertheless, we found that diffusion coefficients in basal and apical membranes have opposite trends on Vn and Fn coating and that anomality coefficients parallel diffusion coefficients (i.e., slower diffusion and higher anomality). Thus, the interaction with immobile Vn in the matrix directing the accumulation of uPAR dimers at the basal membrane increases restriction to local diffusion of the receptors (Fig. 10 A).

We also show that binding to matrix Vn and endocytosis mediated by the uPA–PAI1 complex reversibly regulate the oligomerization state of uPAR. uPA–PAI1 depletes dimers from the cell membrane and, although counteracting cell adhesion,

slows down and restricts the diffusion of uPAR in regions of the apical side (Fig. 10 B). Deviations from the free diffusion of GPI-anchored proteins have recently been explained by a dynamic partition mechanism by which the GPI proteins diffuse into and out of permeable microdomains and are only transiently confined in the absence of molecular cross-linking (Lenne et al., 2006). However, whether or not the interaction of uPAR with either Vn or uPA–PAI1 increases the residence time of the receptor in membrane microdomains to different extents (Kusumi and Suzuki, 2005) is unclear at this point, and it does not appear to be relevant to the issue of uPAR dimerization.

Our results underscore that cell surface protein assemblies, which involve physiological relevant ligands such as Vn and the inhibitor complex uPA–PAI1, play a major role in regulating the diffusion dynamics, oligomerization state, and localization of uPAR at the cell surface. HEK293 cells expressing uPAR are highly motile on Vn (Madsen et al., 2007), and, as cell migration requires the coordination of adhesive and de-adhesive steps, monomer–dimer dynamics may ensure a regulated change in the physical properties of the membrane, modulating contact between the cell and matrix, thus allowing coordinated motion.

These data provide a first example of how the membrane distribution, diffusion, and oligomerization state of a functional GPI-anchored receptor are determined by functionally relevant protein–protein interactions. Because the general physical properties of uPAR are not different from those of other GPI-anchored proteins, our work underscores the importance of using GPI proteins as active sensors rather than as simple reporters of membrane dynamics at the single-molecule level.

## Materials and methods

**Fluorescent protein–tagged uPAR and cell culture**

Expression vectors encoding EGFP- and mRFP1-tagged uPAR were constructed using conventional cloning procedures by inserting the fluorescent protein regions between the third domain of uPAR (D3) and the GPI-anchoring signal. To avoid possible artifacts caused by intrinsic dimerization of the EGFP moiety, a monomeric variant was used (Zacharias et al., 2002). The expression vectors, which were based on the pEGFP-N1 (Clontech Laboratories, Inc.) backbone, were transfected into HEK293 and stable clones isolated by G418 selection and limited dilution. The expression level was measured by flow cytometry, and the number of receptors was measured by binding assays using $Eu^{3+}$-labeled pro-uPA. The clone used in FCS and PCH experiments expressed $12 \pm 2 \times 10^4$ receptors/cell. For FLIM experiments, cells were generated by cotransfecting uPAR-G and uPAR-R expression vectors followed by G418 selection. This pool was not subcloned. All cells were cultured at 37°C and 5% $CO_2$ in high glucose DME, 10% FBS, 5 mM glutamine, 100 U/ml penicillin, and 100 mg/ml streptomycin. Cells plated in glass-bottom 35-mm wells (WillCo) were used at subconfluence (except for Vn and Fn adhesion experiments). uPA–PAI1 stock solution was diluted in medium (2 ml/well) at the final concentration of 8 nM. Cells were incubated for 30 min at 37°C at 5% $CO_2$ and left in the presence of the ligand during data acquisition. For recycling, after incubation with uPA–PAI1, cells were PBS washed and left for 2 h at 37°C and 5% $CO_2$ in fresh medium. EGFP recombinant was a gift of M. Levi (University of Colorado, Boulder, CO). All cell culture reagents were purchased from Invitrogen.

**Spectroscopy and microscopy**

For FCS and PCH, the dual-channel confocal fluorescence correlation spectrometer (ALBA; ISS Inc.,) was equipped with avalanche photodiodes (SPCM-AQR-15; PerkinElmer) and interfaced to an inverted microscope (TE300; Nikon). A 60× 1.2 NA plan Apo water-immersion objective was used. An optical filter (BG39; Chroma Technology Corp.) was placed before the ALBA unit. A mode-locked titanium-sapphire laser (Tsunami; Spectra-Physics) provided two-photon excitation at 920 nm. Every day, the power of the light through the objective in the absence of any immersion liquid was adjusted at 1 mW. An x,y,z computer-controlled piezoelectric actuator with a step resolution of <50 nm (MadCity Lab) warranted the nanometric positioning. An acquisition card (ISS Inc.) received the datastream from the detectors. Data were stored and processed by VISTA (ISS Inc.) and simFCS (Laboratory for Fluorescence Dynamics). Acquisition was in time mode, and sampling frequency was 20 kHz. The waist ($\omega_0$) of the excitation beam was calibrated before each day's experiments by measuring the ACF of 10 nM fluorescein/0.01M NaOH (Invitrogen) using a coefficient of 300 $\mu m^2/s$ (Muller et al., 2003). Typical $\omega_0$ values were 0.35–0.41 $\mu m$; thus, the effective volume as obtained from the Gaussian-Lorentian fit (Muller et al., 2003) was 0.08 $\mu m^3$ (±9%). Local PCH analysis was performed according to Chen et al. (2002) for avoiding the known issue of the overestimation of brightness in live cells. Accordingly, fluorescence intensity traces were subdivided into 2.5-s time intervals, and the histogram of the photon distribution in each interval was evaluated to derive the number of molecules in the observation volume ($n$) and the brightness (i.e., number of detected photons per molecule per second; Chen et al., 1999). Thus, the relative frequency of brightness was obtained from 120 PCHs on each fluorescence intensity trace.

The two-photon excitation scanning fluorescence microscope for the FLIM experiments was assembled at the Laboratory for Fluorescence Dynamics and was described previously (Berland et al., 1995). In summary, 100-fs pulses from a Tsunami mode-locked titanium-sapphire laser were used for excitation. The laser was guided into the microscope by x-y galvano-scanner mirrors (model 6350; Cambridge Technology) driven in a raster scan movement using the three-axis card (ISS Inc.) and synchronized with data acquisition with the Becker and Hickl SPC830 card operating in the FIFO mode, which allows transfer of the delay time of each photon with respect to the laser pulse and the time of arrival of the photon with respect to the beginning of the experiment. At the beginning of the frame, the SPC830 card is armed. Data collection continues until the end of the frame is reached. During this time, data are continuously transferred to the computer memory. At the end of the frame, each photon is associated with a pixel of the image according to the time of arrival with respect to the beginning of frame acquisition. Because the scanner operates synchronously, each photon is accurately positioned in the image. Also, the delay time of each photon with respect to the laser pulse is memorized in a 256-bin histogram at each pixel. Images were collected in 256 × 256 pixel format with a pixel residence time of 100–200 μs, depending on the experiment. Total frame acquisition time was 7–14 s. Several frames (10–30) were acquired and averaged. Data were acquired and processed by simFCS software. A photomultiplier tube (HC120-08; Hamamatsu) was used for detection in the photon-counting mode. An optical filter (BG39) was placed before the photomultiplier. A 40× 1.2 NA water-immersion objective was used (Carl Zeiss, Inc.). The excitation wavelength was 905 nm. The scan area (256 × 256 pixels) corresponds to 32 × 32 $\mu m^2$. Before measurement, a slide with concentrated fluorescein, pH 9.0, was measured. The lifetime of fluorescein, 4.04 ns, was determined separately in a photon-counting spectrofluorometer (PC1; ISS Inc.).

**Statistical analysis**

One-way analysis of variance was performed with Prism software (GraphPad).

**Construction of expression vectors**

The expression vector for uPAR-G was generated by assembling the following fragments in XhoI–XbaI-digested pEGFP-N1 (Clontech Laboratories, Inc.): the signal peptide and extracellular domains of uPAR (residues 20–274) through the amplification of human uPAR cDNA (Roldan et al., 1990) with primers p1U/p2DNX and digested XhoI–NcoI; a sequence encoding monomeric EGFP obtained by amplification with primers p3UEN/p3DHX and digested NcoI–HindIII; and the GPI-anchoring signal of uPAR (residues 276–411) generated by amplifying the uPAR cDNA with oligonucleotides p4U/p4D and digested HindIII–XbaI. The resulting vector encodes a chimeric receptor in which the EGFP coding sequence has been inserted between the third domain of uPAR and the GPI-anchoring signal. The cDNA encoding monomeric EGFP (carrying an Ala207Lys substitution; Zacharias et al., 2002) was generated by site-directed mutagenesis of pEGFP-N1 (Clontech Laboratories, Inc.) using oligonucleotides A207Kf and A207Kr. The vector encoding uPAR-R was generated in the same way except that the mRFP1 cDNA (provided by R.Y. Tsien, University of California, San Diego, La Jolla, CA) was amplified with primers mRFPup/mRFPdo. Before amplification, an internal NcoI site in the mRFP1 sequence was destroyed by silent site-directed mutagenesis using the oligonucleotide pair c420tup/c420tdo.

**Oligonucleotide sequences**
The oligonucleotide sequences used in this study are as follows: p1U (5′-GCGCACTCGAGCTGCCCTCGCGACAT-3′), p3UEN (5′-CGGAATC-CACCATGGTGAGCAAGG-3′), p3DHX (5′-TGCTCTAGATTAAAGCTTGT-ACAGCTCGTCC-3′), p4U (5′-GACCTGGATGTCCAGTACCGCAGT-3′), p4D (5′-GGGATTTCTAGATTAGGTCCAGAGGAG-3′), p2DNX (5′-TGCTCTAG-ATTAATCCATGGGGTGGTTACAGCCACT-3′), A207Kf (5′-CTGAGCACC-CAGTCCAAACTGAGCAAAGACCCC-3′), A207Kr (5′-GGGGTCTTTGC-TCAGTTTGGACTGGGTGCTCAG-3′), mRFPup (5′-CGGGATCCACCGGT-CGCCACCATGGCCTCCTCCGAGGAC-3′), mRFPdo (5′-CCCAAGCTTG-TACAGGGCGCCGGTGGAGTGGCG-3′), c420tup (5′-ATGCAGAAGAA-GACTATGGGCTGGGAGGCC-3′), and c420tdo (5′-GGCCTCCCAGCC-CATAGTCTTCTTCTGCAT-3′).

**uPA-binding assays**
$10^5$ cells were seeded in duplicate wells in complete medium in black 96-well tissue culture plates (Thermo Fisher Scientific) 24 h before the assay. The medium was aspirated, and the cells were incubated for 2 h at 4°C with 50 µl binding buffer (DME, 25 mM Hepes, pH 7.5, and 0.1% BSA) containing increasing concentrations of Europium-labeled pro-uPA[$Eu^{3+}$]. Free pro-uPA[$Eu^{3+}$] was removed by washing twice with binding buffer and once with PBS. After a 15-min incubation in Delfia Enhancement solution (100 µl/well; PerkinElmer), the bound pro-uPA[$Eu^{3+}$] was quantified by time-resolved fluorescence on a Victor 3 system using the Delfia protocol. Specific binding was calculated by subtracting the binding observed to nontransfected HEK293 cells incubated with the same concentrations of pro-uPA[$Eu^{3+}$]. Kd and Bmax were calculated from the binding curves by nonlinear regression analysis using Prism 4 software (GraphPad). Best fits were always obtained assuming a single type of binding site. The number of binding sites per cell was calculated after counting the number of cells present in separate wells.

**Plasminogen activation assays**
HEK293 cells expressing the different receptor variants were tested for plasminogen activation activity using a colorimetric assay. The cells were seeded in complete DME medium at 1,500 cells/well in a 96-well plate 48 h before the assay. The medium was then aspirated, and the cells were incubated in fresh complete DME medium with or without 3 nM uPA for 1 h at 4°C. After this incubation, the cells were washed twice with DME and incubated for 1 h at 37°C in the presence of 0.025 UI/ml human plasminogen (Sigma-Aldrich) and a specific substrate of plasmin, 0.3 mM Chromozyme PL (Roche). The subsequent color development was quantified at 405 nm in an ELISA plate reader.

**Cell adhesion assays**
96-well tissue culture plates were coated with 1 µg/ml Vn, 10 µg/ml Fn, or 100 µg/ml poly-L-lysine in PBS for 2 h at 37°C or overnight at 4°C. Remaining binding sites were saturated by incubation with 2% BSA in PBS for 1 h at 37°C. Immediately before the adhesion assay, cells were washed twice in DME containing 0.1% BSA and resuspended in the same medium at a density of $3 \times 10^6$/ml. 100 µl of cell suspension was added to the wells. Adhesion was allowed to proceed in a humidified incubator at 37°C for 30 min. At the end of the incubation, the wells were washed with 37°C warm DME to remove nonadherent cells. Adherent cells were fixed for 10 min at room temperature with 3% (wt/vol) PFA in PBS and stained for 20 min with 50 µl of a crystal violet solution (0.5% [wt/vol] in 20% methanol). After washing of the plate by immersion in distilled water, the cells were lysed in 1% SDS, and the absorption at 540 nm was measured in an ELISA plate reader. To obtain a measure for specific adhesion, the value obtained from BSA-coated wells was subtracted.

**The phasor transformation**
The *s* and *g* coordinates in the phasor plot corresponding to a given decay, *I(t)*, are given by the following expressions:

$$g_{i,j}(\omega) = \int_0^\infty I_{i,j}(t)\cos(\omega t)dt \,/\, \int_0^\infty I_{i,j}(t)dt \text{ and}$$
$$s_{i,j}(\omega) = \int_0^\infty I_{i,j}(t)\sin(\omega t)dt \,/\, \int_0^\infty I_{i,j}(t)dt,$$

where $\omega$ is the laser repetition angular frequency or the angular frequency of light modulation, and the indexes *i* and *j* identify a pixel of the image. If the data are measured in the frequency domain, then

$$g_{i,j}(\omega) = m_{i,j}\cos(\varphi_{i,j}) \text{ and}$$
$$s_{i,j}(\omega) = m_{i,j}\sin(\varphi_{i,j}), \quad (1)$$

where $m_{i,j}$ and $\varphi_{i,j}$ are the modulation and the phase of the emission with respect to the excitation. If the decay is single exponential, $I(t) = Ae^{-t/\tau}$, the coordinates of the phasor are given by

$$g_{i,j}(\omega) = \frac{1}{1+(\omega\tau)^2} \text{ and}$$
$$s_{i,j}(\omega) = \frac{\omega\tau}{1+(\omega\tau)^2}.$$

In the case in which in a pixel, *i,j*, we have the contribution of several exponential components, the coordinates of the phasor are given by

$$g_{i,j}(\omega) = \sum_k \frac{f_k}{1+(\omega\tau_k)^2} \text{ and}$$
$$s_{i,j}(\omega) = \sum_k \frac{f_k\omega\tau_k}{1+(\omega\tau_k)^2},$$

where $f_k$ is the intensity-weighted fractional contribution of the component with lifetime $\tau_k$. According to the expressions for the coordinate of a phasor for a single exponential decay, $s_{i,j}^2 + (g_{i,j} - 1/2)^2 = 1/2$, which implies that all single exponential components are represented by a semicircle of center (1/2, 0) and radius 1/2 in the phasor plot. We name this the universal circle. On this circle, a phasor corresponding to a very short lifetime (small phase angle) is close to the point (1, 0), whereas a phasor corresponding to a very long lifetime will be close to the (0, 0) point.

**Online supplemental material**
Fig. S1 shows the characterization uPAR-G versus wt-uPAR expressed in HEK293 cells. Fig. S2 illustrates the fitting of a typical ACF by three diffusion models, demonstrating that only the anomalous diffusion model is acceptable. Fig. S3 shows the heterogeneous coexpression of uPAR-G and uPAR-R in live HEK293/GR cells, the pool on which FRET-FLIM was performed. Table S1 lists the results of the statistical analysis on all diffusion coefficients and FRET efficiency data collected in the absence of the inhibitor complex uPA–PAI1. Online supplemental material is available at http://www.jcb.org/cgi/content/full/jcb.200702151/DC1.

We thank Susana Sanchez, Theodore L. Hazlett, and Giuseppe Chirico for advice and Kai Simons for critical review of the manuscript. We are grateful to Beniamino Barbieri, Shih Chu Liao, and Tiefeng You (ISS Inc.) for their support and collaboration. We thank Parijat Sengupta and Davide Gaudesi for technical help and Olga Barreiro del Rio for the valuable discussion. Conventional confocal facilities were provided by Alembic at the San Raffaele Institute.

V.R. Caiolfa and F. Blasi acknowledge support from the Italian Ministry of Education, University, and Research (grants FirbRBAU01CHJJ_002 and FirbRBAU01K532_002). V.R. Caiolfa and N. Sidenius are grateful to the Cariplo Foundation for cofunding this project. The Laboratory for Fluorescence Dynamics is funded by the National Institutes of Health (grant P41 P41-RRO3155) and by the University of California, Irvine.

Submitted: 22 February 2007
Accepted: 2 November 2007

## References

Banks, D.S., and C. Fradin. 2005. Anomalous diffusion of proteins due to molecular crowding. *Biophys. J.* 89:2960–2971.

Berland, K.M., P.T. So, and E. Gratton. 1995. Two-photon fluorescence correlation spectroscopy: method and application to the intracellular environment. *Biophys. J.* 68:694–701.

Blasi, F., and P. Carmeliet. 2002. uPAR: a versatile signalling orchestrator. *Nat. Rev. Mol. Cell Biol.* 3:932–943.

Busso, N., S.K. Masur, D. Lazega, S. Waxman, and L. Ossowski. 1994. Induction of cell migration by pro-urokinase binding to its receptor: possible mechanism for signal transduction in human epithelial cells. *J. Cell Biol.* 126:259–270.

Campbell, R.E., O. Tour, A.E. Palmer, P.A. Steinbach, G.S. Baird, D.A. Zacharias, and R.Y. Tsien. 2002. A monomeric red fluorescent protein. *Proc. Natl. Acad. Sci. USA*. 99:7877–7882.

Chaurasia, P., J.A. Aguirre-Ghiso, O.D. Liang, H. Gardsvoll, M. Ploug, and L. Ossowski. 2006. A region in urokinase plasminogen receptor domain III

controlling a functional association with alpha5beta1 integrin and tumor growth. *J. Biol. Chem.* 281:14852–14863.

Chen, Y., J.D. Muller, P.T. So, and E. Gratton. 1999. The photon counting histogram in fluorescence fluctuation spectroscopy. *Biophys. J.* 77:553–567.

Chen, Y., J.D. Muller, Q. Ruan, and E. Gratton. 2002. Molecular brightness characterization of EGFP in vivo by fluorescence fluctuation spectroscopy. *Biophys. J.* 82:133–144.

Clayton, A.H., Q.S. Hanley, and P.J. Verveer. 2004. Graphical representation and multicomponent analysis of single-frequency fluorescence lifetime imaging microscopy data. *J. Microsc.* 213:1–5.

Conese, M., and F. Blasi. 1995. Urokinase/urokinase receptor system: internalization/degradation of urokinase-serpin complexes: mechanism and regulation. *Biol. Chem. Hoppe Seyler*. 376:143–155.

Cubellis, M.V., T.C. Wun, and F. Blasi. 1990. Receptor-mediated internalization and degradation of urokinase is caused by its specific inhibitor PAI-1. *EMBO J.* 9:1079–1085.

Cunningham, O., A. Andolfo, M.L. Santovito, L. Iuzzolino, F. Blasi, and N. Sidenius. 2003. Dimerization controls the lipid raft partitioning of uPAR/CD87 and regulates its biological functions. *EMBO J.* 22:5994–6003.

Digman, M., V.R. Caiolfa, M. Zamai, and E. Gratton. 2007. The Phasor approach to fluorescence lifetime imaging analysis. *Biophys. J.* doi:10.1529/biophysj.107.120154.

Gratton, E., D.M. Jameson, and R.D. Hall. 1984. Multifrequency phase and modulation fluorometry. *Annu. Rev. Biophys. Bioeng.* 13:105–124.

Gyetko, M.R., R.F. Todd III, C.C. Wilkinson, and R.G. Sitrin. 1994. The urokinase receptor is required for human monocyte chemotaxis in vitro. *J. Clin. Invest.* 93:1380–1387.

Kjoller, L. 2002. The urokinase plasminogen activator receptor in the regulation of the actin cytoskeleton and cell motility. *Biol. Chem.* 383:5–19.

Kusumi, A., and K. Suzuki. 2005. Toward understanding the dynamics of membrane-raft-based molecular interactions. *Biochim. Biophys. Acta*. 1746:234–251.

Lenne, P.F., L. Wawrezinieck, F. Conchonaud, O. Wurtz, A. Boned, X.J. Guo, H. Rigneault, H.T. He, and D. Marguet. 2006. Dynamic molecular confinement in the plasma membrane by microdomains and the cytoskeleton meshwork. *EMBO J.* 25:3245–3256.

Liu, D., J. Aguirre Ghiso, Y. Estrada, and L. Ossowski. 2002. EGFR is a transducer of the urokinase receptor initiated signal that is required for in vivo growth of a human carcinoma. *Cancer Cell*. 1:445–457.

Madsen, C.D., G.M. Ferraris, A. Andolfo, O. Cunningham, and N. Sidenius. 2007. uPAR-induced cell adhesion and migration: vitronectin provides the key. *J. Cell Biol.* 177:927–939.

Mayor, S., and H. Riezman. 2004. Sorting GPI-anchored proteins. *Nat. Rev. Mol. Cell Biol.* 5:110–120.

Muller, J.D., Y. Chen, and E. Gratton. 2003. Fluorescence correlation spectroscopy. *Methods Enzymol.* 361:69–92.

Nykjaer, A., C.M. Petersen, B. Moller, P.H. Jensen, S.K. Moestrup, T.L. Holtet, M. Etzerodt, H.C. Thogersen, M. Munch, P.A. Andreasen, et al. 1992. Purified alpha 2-macroglobulin receptor/LDL receptor-related protein binds urokinase·plasminogen activator inhibitor type-1 complex. Evidence that the alpha 2-macroglobulin receptor mediates cellular degradation of urokinase receptor-bound complexes. *J. Biol. Chem.* 267:14543–14546.

Nykjaer, A., M. Conese, E.I. Christensen, D. Olson, O. Cremona, J. Gliemann, and F. Blasi. 1997. Recycling of the urokinase receptor upon internalization of the uPA:serpin complexes. *EMBO J.* 16:2610–2620.

Odekon, L.E., F. Blasi, and D.B. Rifkin. 1994. Requirement for receptor-bound urokinase in plasmin-dependent cellular conversion of latent TGF-beta to TGF-beta. *J. Cell. Physiol.* 158:398–407.

Paladino, S., D. Sarnataro, R. Pillich, S. Tivodar, L. Nitsch, and C. Zurzolo. 2004. Protein oligomerization modulates raft partitioning and apical sorting of GPI-anchored proteins. *J. Cell Biol.* 167:699–709.

Patterson, G.H., D.W. Piston, and B.G. Barisas. 2000. Forster distances between green fluorescent protein pairs. *Anal. Biochem.* 284:438–440.

Picone, R., E.L. Kajtaniak, L.S. Nielsen, N. Behrendt, M.R. Mastronicola, M.V. Cubellis, M.P. Stoppelli, S. Pedersen, K. Dano, and F. Blasi. 1989. Regulation of urokinase receptors in monocytelike U937 cells by phorbol ester phorbol myristate acetate. *J. Cell Biol.* 108:693–702.

Redford, G.I., and R.M. Clegg. 2005. Polar plot representation for frequency-domain analysis of fluorescence lifetimes. *J. Fluoresc*. 15:805–815.

Resnati, M., I. Pallavicini, J.M. Wang, J. Oppenheim, C.N. Serhan, M. Romano, and F. Blasi. 2002. The fibrinolytic receptor for urokinase activates the G protein-coupled chemotactic receptor FPRL1/LXA4R. *Proc. Natl. Acad. Sci. USA*. 99:1359–1364.

Roldan, A.L., M.V. Cubellis, M.T. Masucci, N. Behrendt, L.R. Lund, K. Dano, E. Appella, and F. Blasi. 1990. Cloning and expression of the receptor for human urokinase plasminogen activator, a central molecule in cell surface, plasmin dependent proteolysis. *EMBO J.* 9:467–474. (published erratum appears in *EMBO J.* 1990. 9:1674)

Sbalzarini, I.F., A. Mezzacasa, A. Helenius, and P. Koumoutsakos. 2005. Effects of organelle shape on fluorescence recovery after photobleaching. *Biophys. J.* 89:1482–1492.

Schwille, P., J. Korlach, and W.W. Webb. 1999. Fluorescence correlation spectroscopy with single-molecule sensitivity on cell and model membranes. *Cytometry*. 36:176–182.

Sidenius, N., A. Andolfo, R. Fesce, and F. Blasi. 2002. Urokinase regulates vitronectin binding by controlling urokinase receptor oligomerization. *J. Biol. Chem.* 277:27982–27990.

Simons, K., and D. Toomre. 2000. Lipid rafts and signal transduction. *Nat. Rev. Mol. Cell Biol.* 1:31–39.

Suhling, K., J. Siegel, D. Phillips, P.M. French, S. Leveque-Fort, S.E. Webb, and D.M. Davis. 2002. Imaging the environment of green fluorescent protein. *Biophys. J.* 83:3589–3595.

Wei, Y., D.A. Waltz, N. Rao, R.J. Drummond, S. Rosenberg, and H.A. Chapman. 1994. Identification of the urokinase receptor as an adhesion receptor for vitronectin. *J. Biol. Chem.* 269:32380–32388.

Wei, Y., M. Lukashev, D.I. Simon, S.C. Bodary, S. Rosenberg, M.V. Doyle, and H.A. Chapman. 1996. Regulation of integrin function by the urokinase receptor. *Science*. 273:1551–1555.

Wei, Y., C.H. Tang, Y. Kim, L. Robillard, F. Zhang, M.C. Kugler, and H.A. Chapman. 2007. Urokinase receptors are required for alpha 5 beta 1 integrin-mediated signaling in tumor cells. *J. Biol. Chem.* 282:3929–3939.

Weiss, M., H. Hashimoto, and T. Nilsson. 2003. Anomalous protein diffusion in living cells as seen by fluorescence correlation spectroscopy. *Biophys. J.* 84:4043–4052.

Zacharias, D.A., J.D. Violin, A.C. Newton, and R.Y. Tsien. 2002. Partitioning of lipid-modified monomeric GFPs into membrane microdomains of live cells. *Science*. 296:913–916.